Experiments in Fluids 30 (2001) 448–457 © Springer-Verlag 2001

Linear and nonlinear gravity-capillary water waves with a soluble surfactant

G. S. Lapham, D. R. Dowling, W. W. Schultz

Abstract Naturally occurring soluble-surfactant slicks influence the properties of water waves. This paper describes results from wave tank experiments involving a soluble surfactant, and linear and nonlinear gravity-capillary waves. Instantaneous surface deflections were measured using optical techniques to determine the damping, phase speed, and the frequency content of the waves for wavemaker frequencies from 4 to 22 Hz. Measured linear-wave phase speed and damping agree well with existing theory at surfactant concentrations away from that leading to maximum damping. Under conditions leading to nonlinear waves, an as-yet-unexplained subharmonic wave with one-sixth the wavemaker frequency was found only with soluble surfactant present.

1 Introduction

Surfactants have an affinity for an interface or surface, and they may be soluble or insoluble in the bulk materials forming the interface. For interfaces formed between air and water, common soluble surfactants are soaps, and common insoluble surfactants are oils. Surfactants often change the interface rheology and consequently cannot be ignored in modeling surface behavior. These changes commonly lead to a reduction in the surface tension and increase the capillary wave damping. Although clean or surfactant-free interfaces are often preferred for basic research studies, some level of surfactant contamination is always present in natural systems.

This paper describes an experimental study of gravity-capillary waves on an air–water interface with a soluble surfactant. The interaction of soluble and insoluble surfactants with water waves has intrigued scientists for many centuries (Franklin 1774; Giles 1969) and remains the focus of current research efforts involving synthetic aperture radar imaging of the ocean (Jahne and Riemer 1990; Ochadlick et al. 1992; Onstott and Rufenach 1992; Peltzer et al. 1992). Although many previous studies have involved waves and surfactants on air–water interfaces (Scriven 1960; Levich 1962; Mann and Hansen 1963; Lucassen and Hansen 1967; Miles 1967; Lucassen-Reynders and Lucassen 1969; Hansen and Ahmad 1971; Hedge and Slattery 1971; Edwards et al. 1991; Cini and Lombardini 1981; Cini et al. 1987; Bock 1987; Bock and Mann 1989; Bock 1989a, b; Bock 1991; Bock and Frew 1993), relatively few experimental investigations have involved soluble surfactants (Cini and Lombardini 1981; Cini et al. 1987; Bock 1987; Bock and Frew 1993) even though soluble surfactants are a common constituent of the marine microlayer (Zutic et al. 1981; Bock and Frew 1993). Essentially all experimental soluble surfactant studies have emphasized the wave damping properties of the surfactants, thereby leaving the effects of surfactants on wave propagation speed unreported. Moreover, even fewer experimental studies (perhaps none) have dealt with surfactant behavior when the water waves were steep enough to be nonlinear, only theoretical work has been done (Miles 1988; Joo et al. 1991).

This paper provides new experimental results in these areas by documenting the results of a study of linear and nonlinear gravity-capillary waves. Waves with frequency (f) between 4 and 22 Hz were investigated in a wave tank containing water and the soluble surfactant Triton-X-100 (Union Carbide Chemical & Plastics Co. Inc., St. Louis, Mo.) in mass fraction amounts between 10^{-8} and 10^{-5}.

In the linear-wave regime, results were obtained for both the phase speed and damping. These experimental results are compared with fitted results from the classical theoretical work of Hansen and Ahmad (1971) and extended in Edwards et al. (1991) to include surfactant diffusion to and from the interface. This model includes surface tension (σ), surface elasticity (E), surface viscosity (μ'), and a surface-bulk diffusion parameter (τ). As required, it properly reduces to the familiar Kelvin dispersion relation (Thompson 1871) in the limit as E, μ', $\tau \to 0$. Agreement between theory and experiments is generally good, but is poor at the surfactant concentration that produces maximum wave damping. In addition, contrary to simple expectation, the extent of wave damping is not monotonically related to the concentration of surfactant.

In the nonlinear regime, measured wave damping increases above its linear-wave value, and, unexpectedly, a surfactant-induced wave at one sixth of the wave-maker

Received: 3 September 2000/Accepted: 8 August 2000

G. S. Lapham
Department of Naval Architecture and Marine Engineering
University of Michigan, Ann Arbor, MI 48109-2145, USA

D. R. Dowling (✉), W. W. Schultz
Department of Mechanical Engineering
University of Michigan, Ann Arbor, MI 48109-2121, USA
e-mail: drd@engin.umich.edu

This research was supported by Office of Naval Research grants N00014-93-1-0867 and N00014-94-1-0850

driving frequency is found. Many possible unintentional origins for this subharmonic wave were experimentally investigated but none were found to be responsible. A surfactant–hydrodynamic interaction is the most likely possibility but a full explanation of the phenomenon remains elusive.

The remainder of this paper is organized into four sections. Sect. 2 describes the experimental apparatus and techniques. The linear-wave results are presented in Sect. 3. The nonlinear-wave results and a summary of the attempts to find an explanation for the one-sixth subharmonic wave are given in Sect. 4. A short summary and the conclusions drawn from this research are provided in Sect. 5.

2
Experimental technique

For these investigations, waves were made in a laboratory wave tank. Measurements of frequency f, wavelength λ, and dimensionless amplitude (or wave slope) ka with a = wave amplitude and $k = 2\pi/\lambda$, were used to determine the phase speed, $c = \omega/k$ where $\omega = 2\pi f$, and the damping coefficient, β, of the waves in the tank. For linear harmonic waves, damping is characterized by spatial exponential decay. Thus, ka is proportional to $e^{-\beta x}$, where x is the distance downstream of the wavemaker, so β can be determined from spatially separated measurements of ka. Frequency analyses of ka time-histories were used to identify nonlinear effects.

The main experimental apparatus was a rectangular wave tank 2.54 m long, 0.305 m wide, and 0.18 m deep made from Plexiglas (Rohm and Haas Co.) and equipped with a plunger-type mechanical wavemaker. Vibration isolation was provided between the separate supporting structures for the tank and the wavemaker. The plunger spanned the width of the tank, had a right-triangular cross section, and was crafted according to the theory of Wang (1974). It was placed approximately 0.45 m from one end of the tank, and was oscillated vertically by a moving carriage driven by a variable speed motor. The plunger's acute angle of 27° was typically dipped approximately 1 cm into the undisturbed surfactant–water solutions. The rear of the plunger was vertical. A sixty-tooth gear coupled to the motor's shaft and a magnetic pickup hooked to an electronic counter measured the oscillation frequency to 0.01 Hz. The experiments dealt exclusively with two-dimensional waves with frequencies between 4 and 22 Hz in the gravity-capillary range. The tank depth was sufficient for all waves in these experiments to be considered to propagate in deep water. Waves with frequencies below 4 Hz are essentially gravity dominated and have very little capillary influence. Acceptable two-dimensional waves could not be reliably produced with the available equipment at frequencies above 22 Hz. Measurements of wavelength and wave frequency were made in the middle 1.5 m of the tank. The duration of a typical experiment was about an hour. Front and side schematic views of the experiment are shown in Fig. 1.

The chemical components of the experiments were chosen for ease of handling and to promote repeatability of experiments. Carbon- and particulate-filtered tap water (referred to herein as nominally-clean water) was used for the experiments along with varying amounts of surfactant to achieve four surfactant/water mass fractions: $M = 10^{-8}$, 10^{-7}, 10^{-6}, and 10^{-5}. The molecular weight of Triton-X-100 is 625 g/mole so these mass fractions correspond to solutions with molarity of 1.6×10^{-11}, 1.6×10^{-10}, 1.6×10^{-9}, and 1.6×10^{-8} gmol/l. All of these concentrations are significantly below the critical micelle concentration (CMC) for Triton-X-100, 2.3×10^{-4} gmol/l (Stebe et al. 1991). Measured gravity-capillary wave characteristics differed little from nominally clean water conditions at lower surfactant concentrations, and became nearly independent of surfactant concentration at higher concentrations. Water temperatures were not controlled but were monitored to ±0.5 °C with a T-type thermocouple placed near, but just below, the water surface. Typical water temperatures during an experiment ranged from 5 to 15 °C, but changed by only a degree or two during any individual experiment.

The soluble surfactant used, Triton-X-100, was recommended as a reasonable chemical stand-in for natural

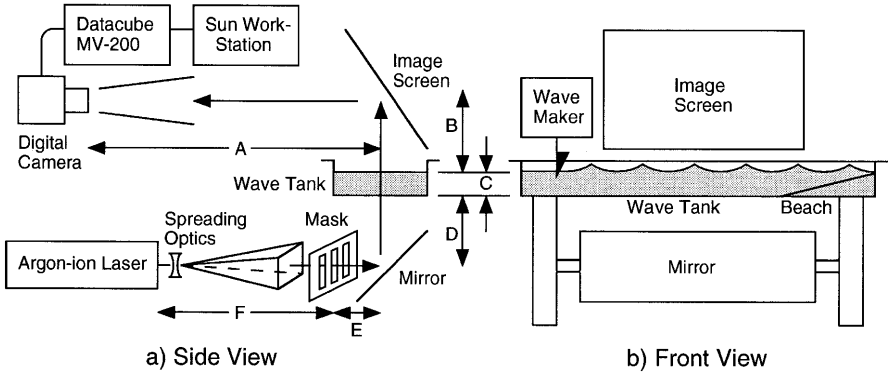

Fig. 1a, b. Schematic drawings of the experimental apparatus: **a** side view, **b** front view. The laser light is spread vertically and horizontally, and then passed upward through the tank and onto the image screen. Shadow-images on the screen produced by the wavy water surface are recorded with a digital camera. The mask is only used in the measurement of temporal ka spectra. Nominal path lengths are: A = 6.35 m, 0.5 m < B < 2.5 m (B was adjusted to achieve the best shadow image), C = 0.18 m, D = 0.27 m, E = 1.16 m, and F = 3.79 m

oceanic surfactants (E. Bock, private communication, 1994). Its viscosity far exceeds that of water, so, to facilitate creation of uniform and repeatable mixtures within the tank, a parent solution of $M = 10^{-3}$ was mixed with the tank water. Unfortunately, the surface properties of aqueous solutions of Triton-X-100 are not completely stable, and the static surface tension of Triton-X-100 solutions varied during our experiments. The annual slide method (Lapham et al. 1999) was used to monitor the static surface tension of the various solutions to ±0.2 dyn/cm. Table 1 lists values for the static surface tension σ, and the temperature-corrected static surface tension changes $\Delta\sigma$ that occurred during these experiments. Although these surface tension changes were consistent, they had little influence on the conduct of the experiments and, whenever necessary, an average value of the surface tension was used in calculations. All experiments were conducted in an ordinary laboratory environment and cleanliness of the facility was maintained by scrupulously washing and flushing the wave tank after every experiment, and by regenerating the parent $M = 10^{-3}$ Triton-X-100 solution each morning. Thus, it was assumed that airborne contamination or slow surface deposition of residual water impurities caused the 0.4 dyn/cm surface tension drop observed during experiments involving surfactant solutions of $M = 10^{-8}$ and nominally-clean water alone.

Wavelengths were determined by standard shadowgraph techniques. The spread beam from an argon–ion laser was passed through the clear plastic tank, through the surfactant solution, and upward out of the wavy air–water interface. A white screen placed above the tank displayed shadow patterns caused by light-ray deflections originating at the air–water interface. The height of the screen above the tank was adjusted to achieve the proper optical sensitivity. A digital camera (Dalsa CA-D1–0256S) with an image field of 256 × 256 pixels running at 225 frames per second (fps) and a framegrabber (Datacube MV-200) collected digital images of the wave-produced shadow patterns for subsequent processing on a Sun Sparcstation-10. The frame rate was sufficient to temporally resolve even the 22 Hz waves. On each frame, eight rows of pixels aligned in the downstream direction and corresponding to the centerline of the tank were averaged and then spectrally analyzed to determine wavelength in pixel dimensions. Data collected from a calibration grid placed at the water surface was used to convert pixel numbers to spatial dimensions. Frame-determined pixel wavelengths were averaged over 16 temporally-separated frames for a final wavelength measurement. The uncertainty of these wavelength measurements depended on the number of waves in the camera's field of view but was estimated to be generally less than ±0.5 mm.

The damping coefficient, β, was determined by fitting a decaying exponential to spatially separated measurements of wave amplitude. Such measurements were made by placing an optical mask with seven vertical slits in the path of the spreading laser beam. The slits formed seven light sheets running in the cross-tank direction that passed through the tank at seven different locations downstream of the plunger. The width of each light sheet at the water surface was approximately 1.5 mm or 14% of the shortest wavelength of this study. When viewed on the screen, the light sheets were seen to oscillate back and forth as water waves propagated on the air–water interface. As for the wavelength measurements, the 225 fps 256 × 256 digital camera was used to make digital movies of the movements of the seven light sheets. Each digital movie had 1024 frames. The movement of each light sheet from its equilibrium location (i.e. location without waves present) is geometrically related to the water-surface slope at the point where the light sheet penetrates the air–water interface. Thus, the recorded movement of the light sheets could be analyzed to determine the temporal spectrum of *ka* at seven different locations downstream of the wavemaker. Spectral amplitudes at the wavemaker frequency were then fit to a decaying exponential to determine the damping coefficient β. For most experiments, the surfactant-induced wave damping was sufficient to quell surface motions before the waves reached the end of the tank. However, wave damping was small for low-frequency (4–6 Hz) waves and nominally clean water conditions, so a simple sloping beach was installed to reduce tank-end wave reflection. The overall accuracy of the damping measurements was approximately ±0.001 mm^{-1}, sufficient to reproduce established clean-water wave-damping results with only modest scatter (see Fig. 2).

Table 1. Basic experimental results and fitting parameters

M	σ (dyn/cm)	$\Delta\sigma$ (dyn/cm)	E (dyn/cm)	μ' (g/s)	τ (s^{-1})
0	73.1	−0.4	0	0	0
10^{-8}	71.1	−0.4	2.2	0.002	0
10^{-7} (low f)	67.4	−0.6	14.0	0.01	0
10^{-7} (high f)	67.4	−0.6	8.0	0.002	0.01
10^{-6}	60.4	−1.1	14.0	0.05	0
10^{-5}	48.0	−2.4	14.0	0.15	0

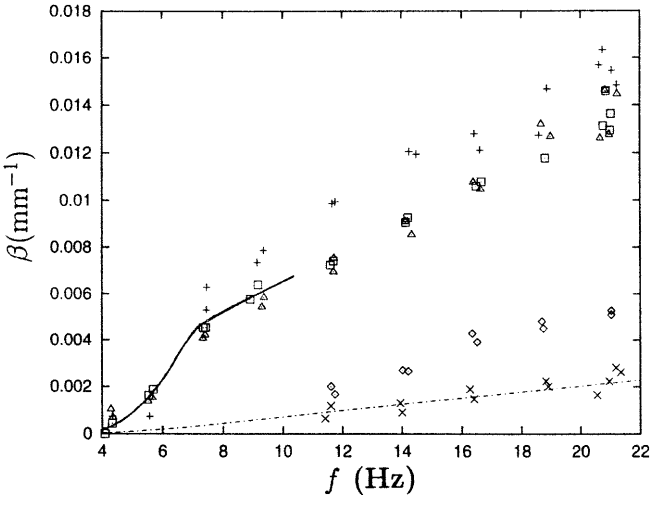

Fig. 2. Measured spatial damping factor, β, as a function of wavemaker frequency, f, for surfactant mass fractions $M = 10^{-8}$(◊), 10^{-7}(+), 10^{-6}(□), 10^{-5}(△), and nominally-clean water (×). The *solid line* is from Cini and Lombardini (1981) at $M = 3.5 \times 10^{-5}$. The *dash–dot line* is the theoretical damping for clean water. Note that the damping does not monotonically increase with surfactant concentration

For the experiments involving nonlinear waves, only temporal amplitude time-histories were recorded. Nonlinear waves were produced by increasing the wave plunger amplitude so that waves on the nominally clean water had amplitudes of $ka \approx 0.1$ in the measurement region of the tank. (Here, k is based on the linear-wave wavelength at the plunger driving frequency.) When surfactant was introduced at these plunger amplitudes, wave amplitudes were typically decreased in the measurement region by an order of magnitude. The temporal spectra computed from these ka time-histories showed the presence of nonlinearity through the development of subharmonic and higher harmonic waves. As discussed in Sect. 4, sideband waves were also observed but these may be related to unintended vibrations of the wavemaker.

A more complete description of the experimental techniques is available in Lapham (1998).

3 Linear waves

In this section, phase speed and damping coefficient results for linear harmonic waves are presented and compared to a theoretical dispersion relationship incorporating surface tension σ, surface elasticity E, surface viscosity μ', and a surface-bulk diffusion parameter τ. For all the experiments reported in this section, ka was less than 0.005. The damping coefficient results are given first since these are more sensitive to the concentration of surfactant.

Fig. 2 displays measured damping coefficient as a function of frequency for the four surfactant solutions of this study (open symbols and +'s) and for nominally-clean water (×'s). On this figure, the dash–dot line is the viscous damping predicted in Lamb (1945) and the solid line is from Cini and Lombardini (1981) at $M = 3.5 \times 10^{-5}$. The data show that the damping coefficient is not a monotonic function of surfactant concentration but instead reaches a maximum for a surfactant concentration near $M = 10^{-7}$ and then falls slightly to a constant value for higher values of M. At high surfactant concentrations, the wave-damping properties of Triton-X-100 apparently saturated and additional surfactant molecules merely remain in the solution or have little additional wave-damping effect on the surface. It should be noted that σ continues to fall with increasing surfactant concentration (see Table 1) even though the damping coefficient has passed its maximum.

Fig. 3 shows the existence of this damping coefficient maximum more explicitly. Here, β is plotted as a function of σ for all experiments conducted within the frequency range $f = 14 \pm 0.3$ Hz. Much of the scatter on this figure is caused by the mismatched frequencies. Nevertheless, β clearly displays a maximum at surface tension values slightly below that of nominally clean water.

The results on the previous figures can be compared directly to the theoretical dispersion relationship of Hansen and Ahmad (1971; see also Edwards et al. 1991). For clarity, these comparisons are done for each of the four M-values of the experiments on the four frames of Fig. 4. For each frame, the measured static surface tension values were used in the calculations. The other parameters were chosen to enhance the fit between the experiments

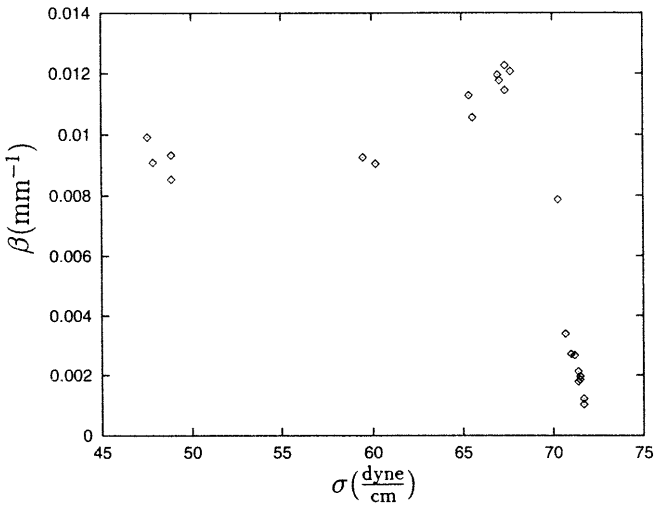

Fig. 3. Measured spatial damping factor, β, as a function of measured static surface tension, σ, for all measurements near 14 Hz. A damping maximum clearly occurs near $\sigma \approx 67$ dyn/cm

and the theory. For, $M = 10^{-8}$, 10^{-6}, and 10^{-5} (Fig. 4a, c, d) the comparisons are reasonable throughout the measured frequency range. Some of the disagreement between the measured and theoretical damping at the highest frequencies may be due to the onset of mild three-dimensional waves at these frequencies. Using the same value of E for the two highest concentration cases is reasonable since the surface elasticity of other soluble surfactants has been shown to be insensitive to surfactant concentration when the surface tension has dropped 10 dyn/cm below the clean water value (Bock and Frew 1993). The $M = 10^{-7}$ (Fig. 4c) case, could not be fit with any single set of parameters (E, μ', τ). Additionally, no combination of these three parameters was found that could produce damping as high as the 8–12 Hz measurements at $M = 10^{-7}$. Two fits that adequately model the low and high frequency ranges of the $M = 10^{-7}$ data are shown on Fig. 4c. Table 1 lists the parameter values for the dispersion relationship calculations shown on Fig. 4.

Although it remains a conjecture at this point, the lack of a consistent theoretical match over the entire frequency range of damping data at $M = 10^{-7}$ may be related to some type of surfactant phase transition. At lower bulk concentrations of Triton ($M < 10^{-7}$), the surface-absorbed molecules may be far apart enough apart to be randomly oriented like a gas. At higher concentrations ($M > 10^{-6}$), the surface-absorbed molecules may be oriented and closely-packed like a solid or randomly aligned but in constant interaction like a liquid. For concentrations near maximum damping ($M \approx 10^{-7}$) the surface-absorbed molecules may be fluctuating between randomly-oriented and closely-packed configurations as the surface waves pass. The molecular time scales associated with these hypothesized changes of configuration may lead to the observed wave-frequency dependence of the damping.

Measured phase speeds are compared to the theoretical dispersion relationship predictions on Fig. 5 where phase speed c is plotted vs. frequency. The curve with the highest phase speed is from the inviscid Kelvin dispersion

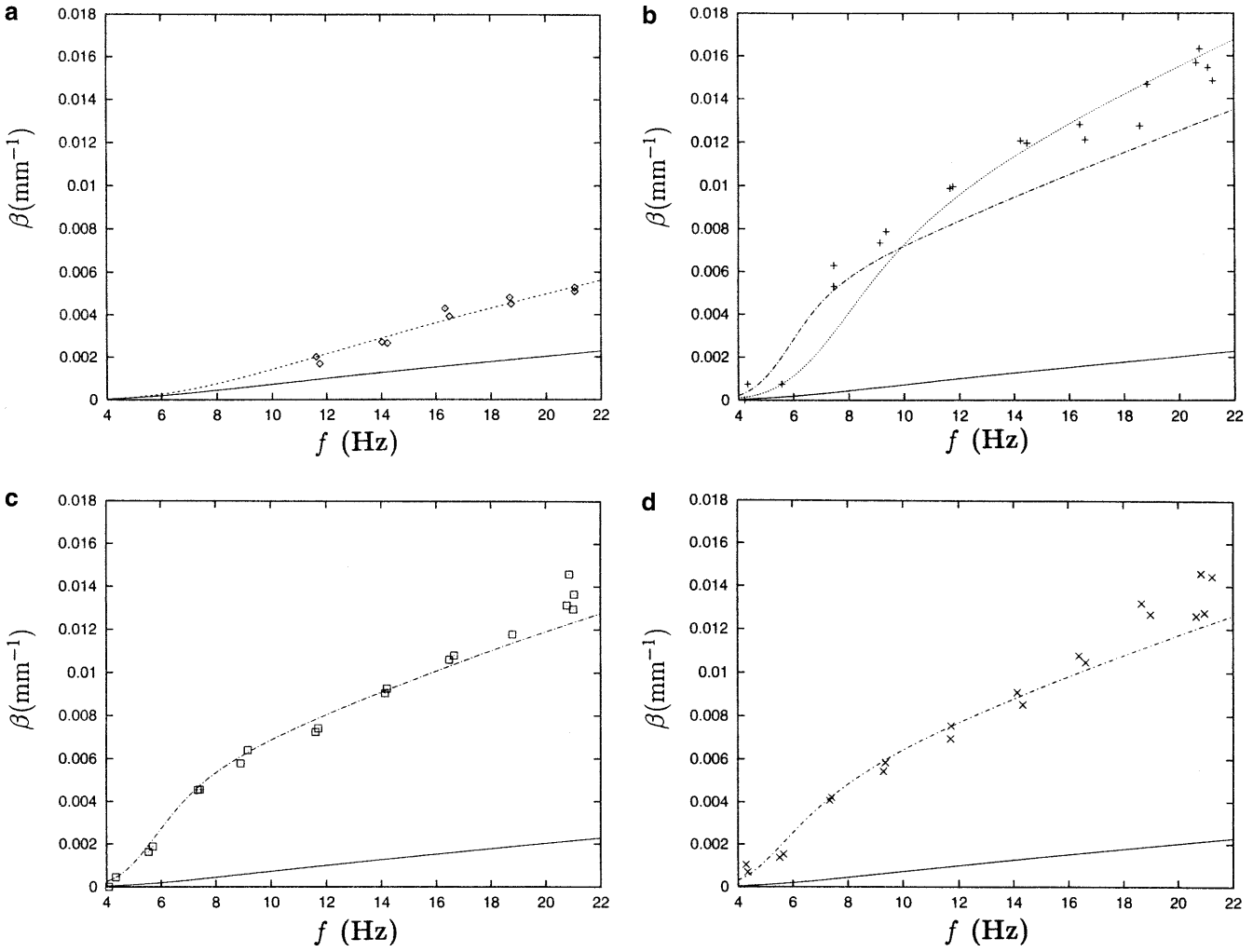

Fig. 4a–d. A comparison of the measured damping to the classical theory of Hansen and Ahmad (1971): **a** $M = 10^{-8}$, **b** $M = 10^{-7}$, **c** $M = 10^{-6}$, **d** $M = 10^{-5}$. Parameters for the theory are listed in Table 1. The measurement in **b** could not be fit by one set of parameters so high- and low-frequency fits are shown. The *solid line* on each frame is the theoretical clean water damping

relationship with $\sigma = 73$ dyn/cm. The other curves are from the Hansen and Ahmad model with all surface rheological parameters deduced from the damping measurements. Note that the theoretical curve for $M = 10^{-8}$ falls on top of the nominally clean water curve to graphical accuracy. The data scatter shown on Fig. 5 is produced by mild variations in the experimental conditions. The main trend shown on Fig. 5 is a monotonic decrease in the phase speed for increasing surfactant concentration. Given the importance of the surface tension dependency in the phase speed of capillary waves ($c^2 = k\sigma/\rho$ as $k \to \infty$), this trend follows the expected monotonic decrease in the surface tension with increasing surfactant concentration. Good agreement between theory and experiment is found for surfactant solutions of $M = 10^{-8}$, 10^{-6}, and 10^{-5}. Theoretical curves from both sets of parameters for the $M = 10^{-7}$ surfactant solutions are plotted on Fig. 5. The low-frequency parameters ($E = 14.0$ dyn/cm, $\mu' = 0.01$ g/s, and $\tau = 0$) plotted as the solid curve on Fig. 5 provide the better fit to the $M = 10^{-7}$ phase-speed data throughout the entire frequency range. The relatively good agreement shown on Fig. 5 suggests that σ, E, and μ' are sufficient to explain phase speeds measurements for Triton-X-100/water solutions in the frequency range of these experiments. However, the damping data suggest additional modeling is needed to predict the behavior of an $M = 10^{-7}$ Triton-X-100/water solution.

4
Nonlinear waves

The damping experiments were repeated with an increase in plunger amplitude to introduce nonlinearity, and measured temporal ka-spectra were examined for the appearance of subharmonic, higher harmonic, and sideband waves. A profound effect was found when surfactant was present and the wavemaker amplitude was large enough to produce waves of $ka \approx 0.1$ in nominally clean water. In addition, a general increase in the wave damping was seen for nonlinear waves.

When the wavemaker was driven between 13 and 20 Hz at $M = 10^{-7}$, two wave trains were produced in the tank: one at the wavemaker driving frequency, and one at one-sixth the driving frequency. The fundamental wave was dominant near the wavemaker while the subharmonic

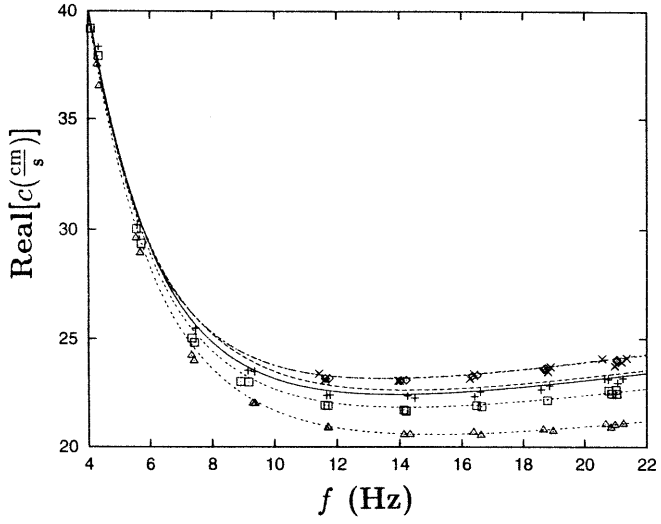

Fig. 5. A comparison of theoretical and measured phase speed, c, (the real part of the dispersion relationship) vs. wavemaker frequency, f, for surfactant mass fractions $M = 10^{-8}(\diamond)$, $10^{-7}(+)$, $10^{-6}(\square)$, $10^{-5}(\triangle)$, and nominally-clean water ($\times$). Kelvin theory for clean water has the highest phase speed, and lies on top of the $M = 10^{-8}$ curve to graphical accuracy. The other curves use the parameters from Table 1 and match the appropriate measurements well. Theoretical curves for both sets of parameters at $M = 10^{-7}$ are shown. The *solid line* fits this data best and corresponds to the low-frequency parameters

wave appeared where the fundamental was heavily damped. Unlike some wave resonances, the two waves were not phase locked in space (the wavelengths are not integer multiples of each other). The frequency ratio between the two waves was found to be exactly one-sixth to within experimental error. Figure 6 shows a plot of the subharmonic frequency, f_s, vs. the fundamental plunger frequency, f_f. The solid line has a slope of 1/6 and the error bars shown are plus-or-minus one half a frequency bin

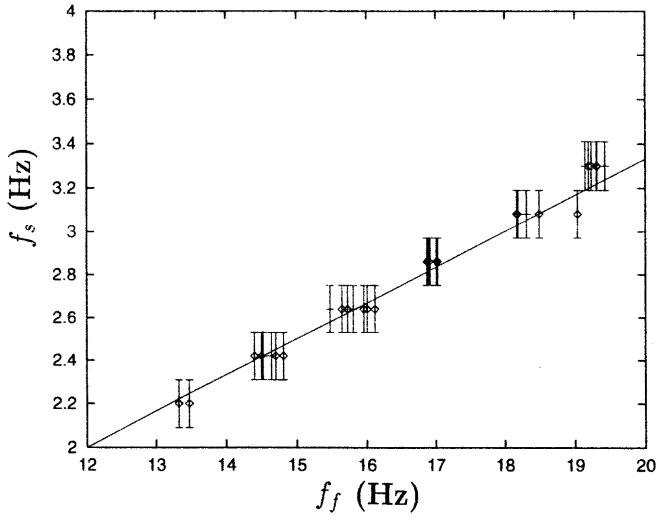

Fig. 6. Measured frequency of the one-sixth subharmonic wave, f_s, vs. the wavemaker fundamental frequency, f_f. The *solid line* has a slope of one-sixth and falls inside of all the *error bars*, which denote plus-or-minus one half the spectral frequency-bin size. Data for both $M = 10^{-7}(\lozenge)$ and $10^{-6}(+)$ are shown

width from the FFT spectra. From an experimental perspective, the fit to the one-sixth line is essentially perfect. An explanation of this phenomenon remains elusive and most of the remainder of this section is devoted to documenting when it occurs.

Once the one-sixth subharmonic was identified, a wide variety of exploratory experiments were undertaken to determine whether it was a genuine surfactant-hydrodynamic phenomenon or merely an experimental artifact. First, the subharmonic wave was definitely not an electronic artifact because it was clearly visible by eye in the shadow patterns produced on the screen above the tank, and spectral analysis of the spatial shadow patterns confirmed this observation. Secondly, the subharmonic wave was absent from nonlinear-wave experiments employing only the nominally clean water or an insoluble monolayer of stearic acid. However, the subharmonic wave was present at Triton-X-100 concentrations from below $M = 10^{-7}$ to slightly above $M = 10^{-6}$, and it could even be produced by replacing the high-purity single-component Triton-X-100 with common dishwashing liquid.

The main difference between soluble and insoluble surfactants lies in the bulk fluid's ability to supply surfactant to a dilating surface or absorb surfactant from a contracting surface for the soluble case. Naturally, these possibilities are absent for the insoluble surfactant. Perhaps the subharmonic wave is generated by surface rheology changes induced when the absorption mechanics between the surface surfactant and the dissolved surfactant in the bulk fluid layer just below the surface are somehow enhanced, modified, or disrupted by the surface stretching and contraction associated with the higher-frequency nonlinear waves produced by the wave maker. The reasons for the occurrence of the one-sixth subharominc are as yet unknown, although they do appear to be connected with the concentration range of maximum wave damping identified in the linear-wave studies presented in Sect. 3.

The presence or lack of the subharmonic wave is best illustrated by comparing temporal *ka* spectra with and without the soluble surfactant. Sample spectra showing the presence of the subharmonic wave (2.83 Hz) are given in Fig. 7 for a fundamental frequency of 16.9 Hz. These spectra were measured at three different distances downstream of the wavemaker: 0.225 m (Fig. 7a), 0.334 m (Fig. 7b), and 0.442 m (Fig. 7c). Note the vertical scale change among frames (a)–(c) on Fig. 7. A summary of the wave amplitude dependence on downstream distance for these two waves is given on Fig. 8. The fundamental wave decays smoothly. The subharmonic wave amplitude does not have a simple trend with increasing downstream distance because the longer subharmonic waves establish a partial standing wave system in the tank. In particular, the second subharmonic wave data point on Fig. 8 is lower than all the others; it is believed to lie near a node of the partial standing wave system at the subharmonic frequency.

Temporal *ka* spectra obtained under identical circumstances without surfactant are quite different. Figure 9 shows nominally clean water spectral results measured at the same three locations as the spectra in Fig. 7 for a fundamental frequency of 17.0 Hz. A direct comparison of

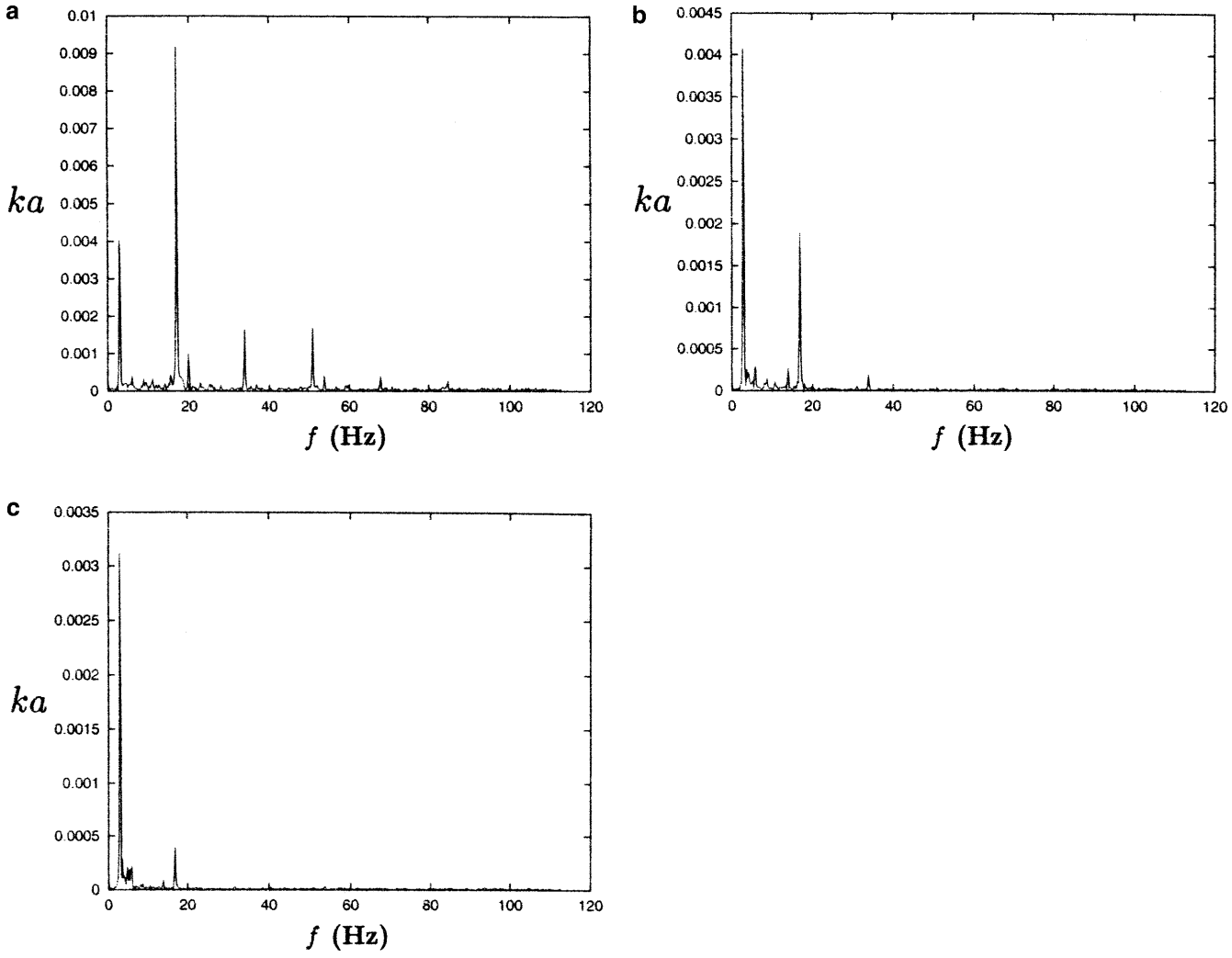

Fig. 7a–c. Temporal spectra of wave amplitude, ka, at $M = 10^{-7}$ and $f_f = 16.9$ Hz measured **a** 225 mm, **b** 334 mm, and **c** 442 mm downstream from the wavemaker. The one-sixth subharmonic occurs at $f_s = 2.86$ Hz

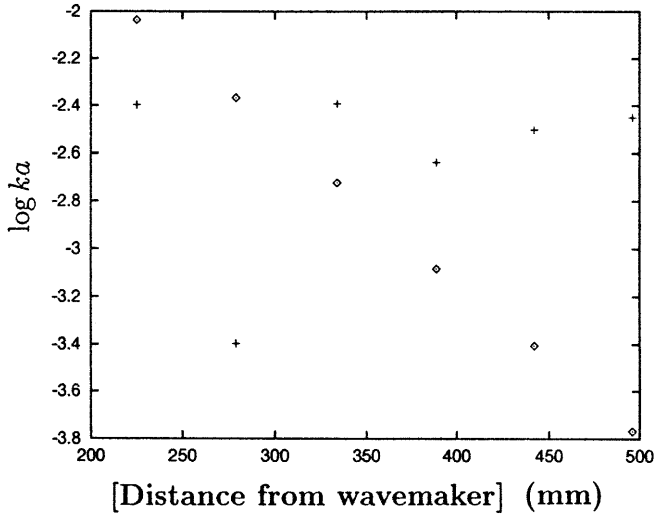

Fig. 8. Wave amplitude vs. distance at $M = 10^{-7}$ and $f_f = 16.9$ Hz for the fundamental wave (◊) and the subharmonic wave (+). The amplitude of the fundamental wave decays exponentially. The amplitude of the unanticipated subharmonic wave varies with downstream distance because it established a partial standing wave system in the tank

Figs. 7 and 9 shows that the nominally clean water waves have larger amplitudes, stronger sidebands, and *typical* higher harmonics but *no* subharmonics. In addition, the one-sixth harmonic wave was not visually apparent in the wave-induced shadow patterns when nonlinear waves were made with nominally clean water alone.

The emergence of the one-sixth subharmonic wave caused some unanticipated experimental difficulties such as reflections from the vertical wall at the end of the tank. As previously explained, these reflections contributed to the observed partial standing wave system at the subharmonic frequency that leads to the non-monotonic subharmonic amplitude results seen on Fig. 8. Thus, the subharmonic wave could have been related to a tank resonance. To determine whether this was a tank-resonance phenomenon, a temporary vertical wall was added to shorten the length of the tank, and a beach was added to change the end-condition of the tank. After both changes, the subharmonic wave phenomenon persisted with nearly the same amplitude, so it was presumed to be independent of the size and configuration of the tank.

The dependence of the subharmonic wave generation mechanism on fundamental wave amplitude was also quite

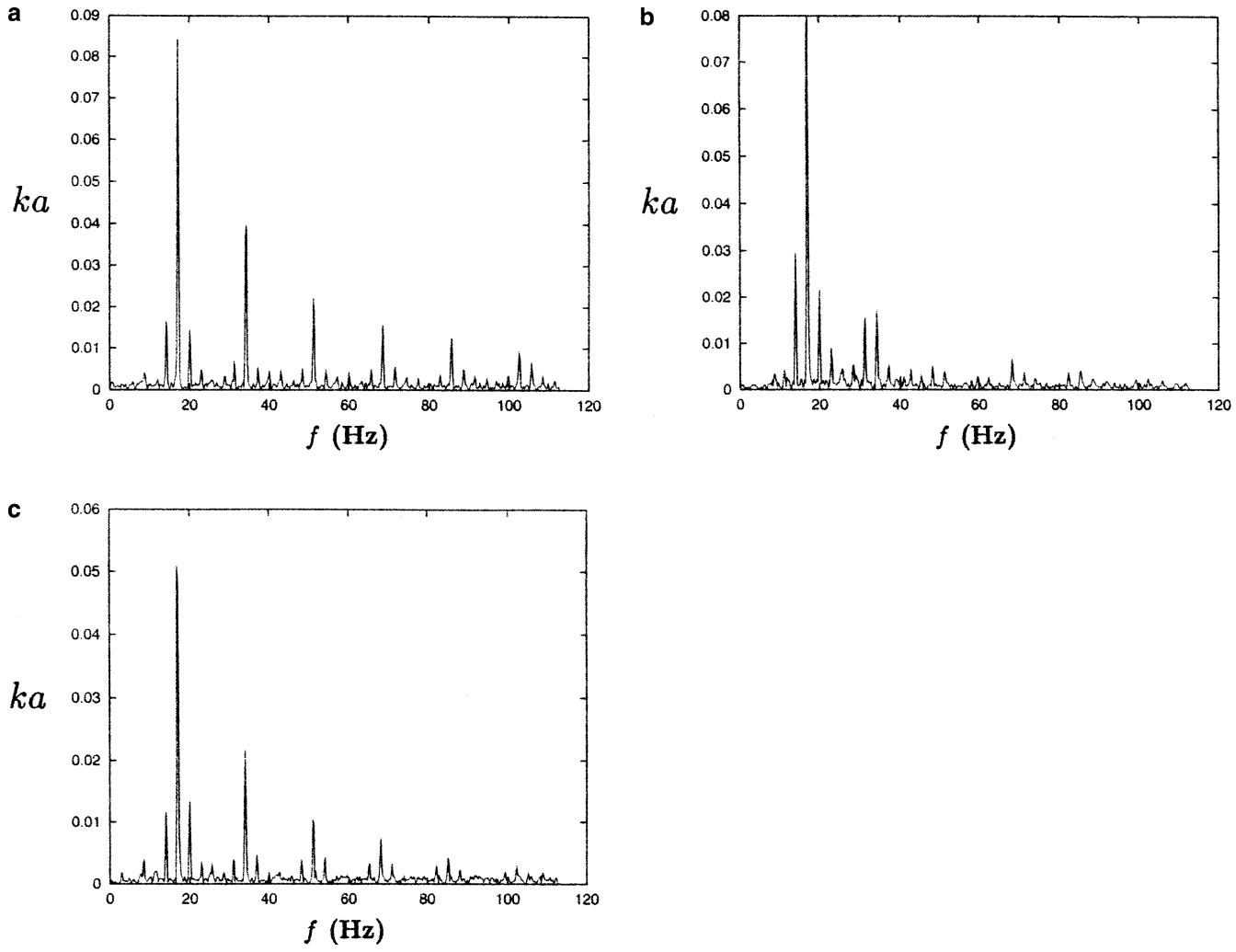

Fig. 9a–c. Temporal spectra of wave amplitude, *ka*, for nominally-clean water at $f_f = 17.0$ Hz measured **a** 225 mm, **b** 334 mm, and **c** 442 mm downstream from the wavemaker. This experiment is identical to the one that produced Fig. 7 except the surfactant is absent. The one-sixth subharmonic wave is absent as well

clear. Many experiments had been done with linear waves in the same frequency range at the same surfactant concentrations without production of the one-sixth subharmonic wave. Thus nonlinearity was required to activate the one-sixth subharmonic.

The possibility that a bulk-flow effect induced by the wavemaker was the source of the one-sixth subharmonic was also investigated and discarded. The tank was seeded with reflecting particles and the region beneath the operating plunger was observed. There was little movement of the particles beneath the wavemaker and no tank-wide circulatory flow was seen.

As a final set of tests to determine the subharmonic wave's origin, an accelerometer was attached to the plunger, and acceleration spectra were collected in all three orthogonal directions while the wavemaker operated at 16.6 Hz in a full tank of surfactant solution of $M = 10^{-7}$. This accelerometer study produced two important findings: (i) the wavemaker did not provide any significant vibrational excitation at one-sixth of the fundamental frequency, and (ii) the sidebands seen in the nominally-clean water temporal spectra (Fig. 9) may be due to unintended wavemaker motions. Thus, it was concluded that the one-sixth subharmonic was not the direct result of unintended plunger motions, although features of the nominally clean water results might be.

The final component of the nonlinear experiments involved measuring changes in damping of the nonlinear waves compared to linear waves. Figure 10 shows the difference between wave damping at plunger amplitude of 0.18 mm (used for all of the linear-wave data) and the damping of waves produced at four-times that plunger amplitude. Both curves are for $M = 10^{-7}$ and the nonlinear-wave damping departs from the linear-wave measurements around 15 Hz. The onset of enhanced damping will clearly depend on a and frequency ($f = kc/2\mathrm{p}$). The two sets of measurements shown on Fig. 10 were made with a constant paddle-oscillation amplitudes so the horizontal axis, in effect, also denotes increasing *ka*. Naturally, as *ka* increases nonlinear effects must become apparent at some point. Here, nonlinearity is seen to only mildly increase the damping, a point that has been previously observed and predicted (Reynolds 1880; Levich 1962; Miles 1967; Joo et al. 1991). The measured increase in nonlinear-

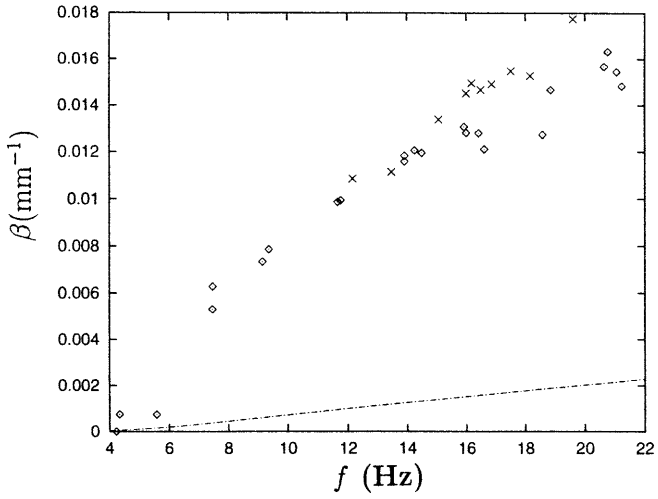

Fig. 10. Linear (◊) and nonlinear (×) damping for a concentration of $M = 10^{-7}$. The plunger amplitude is four times greater for the nonlinear measurements. Damping is slightly increased by nonlinearity. The *dashed line* represents the clean water damping

wave damping does not appear to be related to the presence of the subharmonic wave, since subharmonic waves were found at frequencies as low as 13 Hz where both types of damping measurements coincide. Unfortunately, with the existing apparatus, additional plunger stroke increase lead to three-dimensional waves.

5
Summary and conclusions

The experimental study reported here was undertaken to determine how a soluble surfactant influences both linear and nonlinear gravity capillary waves. Measurements of phase speed and damping coefficient have been made using nonintrusive optical techniques. For linear waves, the major findings of this research generally support existing theoretical models, but they have also identified a need for additional experiments and modeling. For nonlinear waves, an interesting new phenomenon has been found when a soluble surfactant – but not an insoluble stearic-acid – slick is present.

The linear and nonlinear-wave results lead to several conclusions. First, a monotonic relationship between the concentration of surfactant and the extent of wave damping does not exist for Triton-X-100/water solutions. Instead, maximum damping is found at the modest surfactant–water mass fraction of 10^{-7}, far below the CMC. For smaller or larger surfactant concentrations, the existing theory for water wave dispersion on contaminated surfaces is generally quite good. However, near the peak-damping concentration, a single set of surface parameters cannot reproduce the measured behavior. The existence of this unexpected surface behavior is possibly connected to the onset of saturation of surfactant molecules at the air–water interface. Interestingly, any such saturation phenomena is only connected with surface dynamics because the static surface tension of a Triton-X-100/water solution continues to decrease monotonically with increasing surfactant long past the concentration where gravity-capillary wave damping has become constant.

Second, there exists a nonlinear-wave–surfactant interaction that can lead to the production of a one-sixth temporal-subharmonic wave from a fundamental-frequency wave train. This new interaction was shown to persist over a range of fundamental wave frequencies and was determined to not be a direct artifact of the experiment. It is not a subharmonic instability caused from sideband frequencies in the Benjamin–Feir (1967) sense. Rather, it is the development of a frequency peak at one-sixth the frequency of the wavemaker. This surfactant-induced spectral downshifting may be an important oceanic wave-energy transfer mechanism between wind-forced capillary waves having relatively high wavenumbers and lower-wavenumber gravity waves. While the precise origin of the one-sixth subharmonic wave was not identified by this study, several possibilities exist. One source could be a surfactant-induced interaction between Laplace and Marangoni (or longitudinal) waves (Edwards et al. 1991). While the fluid motions of these modes are predominantly perpendicular to each other, they might be coupled through a surface interaction. Interestingly, both types of waves involve surface contraction and dilation, which is of enhanced importance for nonlinear Laplace waves. A second possibility (M. Perlin, private communciation, 1997) is a surfactant-enhanced wave-triad interaction that produces the one-sixth subharmonic wave through a nonlinear coupling of the fundamental wave and unintentional sideband waves produced by the wavemaker. The frequency difference between the fundamental and sideband waves observed in the nonlinear experiments involving the nominally-clean water alone matches, within experimental precision, the frequency of the one-sixth subharmonic produced under the same circumstances when the soluble surfactant is present. Although this triad-interaction explanation may relegate the one-sixth-factor to a special case associated only with the experiments described here, it still requires a new surfactant-induced wave-coupling phenomenon.

And finally, the mildly increased damping rates of nonlinear waves in the presence of surfactants matches previous expectations.

References

Benjamin T; Feir J (1967) The disintegration of wave trains on deep water. J Fluid Mech 27: 417

Bock E (1987) On ripple dynamics: I. Microcomputer-aided measurement of ripple propagation. J Colloid Interface Sci 119: 326

Bock E (1989a) On ripple dynamics: III. Linear propagation of plane-wave packets: theory. J Colloid Interface Sci 129: 561

Bock E (1989b) On ripple dynamics: IV. Linear propagation of plane-wave packets: observation. J Colloid Interface Sci 131: 38

Bock E (1991) On ripple dynamics: V. Linear propagation cylindrical waves on liquids with and without a surface dilational viscoelastic response. J Colloid Interface Sci 147: 422

Bock E; Frew N (1993) Static and dynamic response of natural multicomponent oceanic surface films to compression and dilation: laboratory and field observations. J Geophys Res 98: 14599

Bock E; Mann J (1989) On ripple dynamics: II. A corrected dispersion relation for surface waves in the presence of surface elasticity. J Colloid Interface Sci 129: 501

Cini R; Lombardini P (1981) Experimental evidence of a maximum in the frequency domain of the ratio of ripple attenuation in monolayered water to that of pure water. J Colloid Interface Sci 81: 125
Cini R; Lombardini P; Manfredi C; Cini E (1987) Ripple damping due to monomolecular films. J Colloid Interface Sci 119: 74
Edwards D; Brenner H; Wasan D (1991) Interfacial transport processes and rheology. Butterworth-Heinenmann, Stoneham, Mass
Franklin B (1774) On the stilling of waves by means of an oil. Phil Trans Roy Soc 64: 445
Giles C (1969) Franklin's teaspoon of oil: studies of the early history of surface chemistry. Chem Ind 8: 1616
Hansen R; Ahmad J (1971) Waves at interfaces. In: Danielli J, Rosenberg M, Cadenhead D (eds) Progress in surface and membrane science, vol 4. Academic Press, New York, pp 1–55
Hedge M; Slattery J (1971) Capillary waves at a gas–liquid interface. J Colloid Interface Sci 35: 183
Jahne B; Riemer K (1990) Two dimensional wave number spectra of small-scale water surface waves. J Geophys Res 95: 11531
Joo S; Messiter A; Schultz W (1991) Evolution of weakly nonlinear water waves in the presence of viscosity and surfactant. J Fluid Mech 229: 135
Lamb H (1945) Hydrodynamics, 6th edn. Dover, New York
Lapham G (1998) Wave-surfactant interaction, PhD Thesis, University of Michigan, Ann Arbor
Lapham G; Dowling D; Schultz W (1999) In situ force balance tensiometry. Exp Fluids 17: 157
Levich V (1962) Physiochemical hydrodynamics. Prentice Hall, New York
Lucassen J; Hansen R (1967) Damping of waves on monolayer-covered surfaces. J Colloid Interface Sci 23: 319
Lucassen-Reynders E; Lucassen J (1969) Properties of capillary waves. Adv Colloid Interface Sci 85: 52
Mann J; Hansen R (1963) Propagation characteristics of capillary ripples: III. Capillary ripple velocity and attentuation dispersion on clean water surfaces and on various monolayers. J Colloid Interface Sci 18: 805
Miles J (1967) Surface-wave damping in closed basins. Proc Roy Soc 297A: 459
Miles J (1988) The evolution of a weakly nonlinear, weakly damped, capillary-gravity wave packet. J Fluid Mech 187: 141
Ochadlik A; Cho P; Evans-Morgis J (1992) Synthetic aperture radar observations of currents and colocated slicks. J Geophys Res 97: 5325
Onstott R; Rufenach C (1992) Shipboard active and passive microwave measurement of ocean surface slicks of the southern California coast. J Geophys Res 97: 5315
Peltzer R; Griffin O; Barger W; Kaiser J (1992) High resolution measurement of surface-active film redistribution in ship wakes. J Geophys Res 97: 5231
Reynolds O (1880) On the effect of oil destroying waves on the surface of water. Brit. Assoc. Rept. Papers 1: 409
Scriven L (1960) Dynamics of a fluid interface. Chem Eng Sci 12: 98
Stebe K; Lin S-Y; Mardarelli C (1991) Remobilizing surfactant retarded fluid particle interfaces: I. Stress-free conditions at the interfaces of micellar solutions of surfactants with fast sorption kinetics. Phys Fluids A 3: 3
Thompson W (1871) Hydrokinetic solutions and observations. Phil Mag 42: 368
Wang S (1974) Plunger-type wavemakers: theory and experiment. J Hydraul Res 12: 357
Zutic V; Cosovic B; Marcenko E; Bihari N (1981) Surfactant production by marine phytoplankton. Mar Chem 10: 505